



This is a repository copy of *Adsorption Studies of p-Aminobenzoic Acid on the Anatase TiO₂(101) Surface*.

White Rose Research Online URL for this paper:
<http://eprints.whiterose.ac.uk/81253/>

Version: Submitted Version

Article:

Thomas, A.G., Jackman, M.J., Wagstaffe, M. et al. (5 more authors) (2014) Adsorption Studies of p-Aminobenzoic Acid on the Anatase TiO₂(101) Surface. *Langmuir*, 30 (41). 12306 - 12314. ISSN 0743-7463

<https://doi.org/10.1021/la5032619>

Reuse

Unless indicated otherwise, fulltext items are protected by copyright with all rights reserved. The copyright exception in section 29 of the Copyright, Designs and Patents Act 1988 allows the making of a single copy solely for the purpose of non-commercial research or private study within the limits of fair dealing. The publisher or other rights-holder may allow further reproduction and re-use of this version - refer to the White Rose Research Online record for this item. Where records identify the publisher as the copyright holder, users can verify any specific terms of use on the publisher's website.

Takedown

If you consider content in White Rose Research Online to be in breach of UK law, please notify us by emailing eprints@whiterose.ac.uk including the URL of the record and the reason for the withdrawal request.



eprints@whiterose.ac.uk
<https://eprints.whiterose.ac.uk/>

Adsorption studies of *p*-aminobenzoic acid on the anatase TiO₂ (101) surface.

Andrew G. Thomas^{*1}, Mark J. Jackman^{1,2}, Michael Wagstaffe¹, Hanna Radtke¹, Karen Syres³, Johan Adell⁴, Anna Lévy^{5‡}, and Natalia Martsinovich⁶.

1. School of Materials and The Photon Science Institute, The University of Manchester, Oxford Road, Manchester, M13 9PL, UK.
2. School of Physics and Astronomy, The University of Manchester, Oxford Road, Manchester, M13 9PL, UK.
3. School of Chemistry, The University of Nottingham, University Park, Nottingham NG7 2RD, UK
4. MaxLab, Ole Römers väg 1, 223 63, Lund, Sweden.
5. Synchrotron Soleil, Orme des Merisiers, Saint Aubin, BP 48 - 91192 – Gif-sur-Yvette, France
6. Department of Chemistry, The University of Sheffield, Sheffield S3 7HF, UK.

*Corresponding author.

‡ Current address: Sorbonne Universités, UPMC, Paris 06, CNRS, INSP, UMR 7588, F-75252, Paris Cedex 05, France

Abstract.

The adsorption of *p*-aminobenzoic acid (*p*ABA) on the anatase TiO₂ (101) surface has been investigated using synchrotron radiation photoelectron spectroscopy, Near Edge X-ray Absorption Fine Structure (NEXAFS) spectroscopy and Density Functional Theory (DFT). Photoelectron spectroscopy indicates that the molecule is adsorbed in a bidentate mode through the carboxyl group following deprotonation. NEXAFS spectroscopy and DFT calculations of the adsorption structures indicate ordering of a monolayer of the amino acid on the surface with the plane of the ring in an almost upright orientation. Adsorption of *p*ABA on nanoparticulate TiO₂ leads to a red shift of the optical absorption relative to bare TiO₂ nanoparticles. DFT and valence band photoelectron spectroscopy suggest the shift is attributed to the presence of the highest occupied molecular orbitals in the TiO₂ band gap region and the presence of new molecularly derived states near the foot of the TiO₂ conduction band.

1. Introduction.

The adsorption of organic molecules for the functionalization of titania is of interest for a number of technological applications including photovoltaics¹,

biosensors² and targeted biomaterials³ to name but a few. The interaction of titania with amino acids in particular is interesting, since it is well established that carboxylic acids bond strongly to titania surfaces in a bidentate bridging fashion, following deprotonation of the acid group⁴⁻⁶. The adsorption of amino acids then has relevance in understanding surface interactions in novel biosensors based on TiO₂ and also in the osseointegration of Ti biomaterials, where the active surface is thought to be the native oxide⁷. The adsorption of amino acids on TiO₂ surfaces via the carboxyl group is thought to leave the amine group unbound⁸⁻¹⁰. The free amine group could then be used to graft polymers or biomolecules onto TiO₂ for biosensing¹¹, or novel biomaterial applications^{3,12}. In addition, the free amine group could be used to anchor light-harvesting quantum dots, such as CdSe or PbS, to the TiO₂ surface¹³. The formation of a strong bond between the light-sensitizer and n-type material is thought to be important in allowing efficient charge transfer between the two materials in photovoltaics. Recently there have been a number of studies on CdSe and PbS quantum dots, which suggest they exhibit multiple exciton generation, i.e. the production of more than one exciton for each absorbed photon. It has also been shown that charge transfer does occur between these quantum dots and TiO₂ single crystal surfaces¹⁴. Cysteine linker molecules have been shown to enhance the efficiency of charge transfer between CdSe quantum dots and nano-structured TiO₂ surfaces relative to mercaptopropionic acid and thioglycolic acid linkers¹³. One might expect that an aromatic amino acid such as *p*-aminobenzoic acid (pABA) (see figure 1) may further enhance this effect due to the delocalization in the phenyl ring. The aromatic ring offers resonance structures for electron or hole trapping. This trapping, it has been suggested, can lead to an increase in the rate and efficiency of charge transfer when using cysteine as a linker molecule for CdSe quantum dots on nanostructured TiO₂ surfaces¹³.

Furthermore, pABA, like pyrocatechol (benzene-1,2-diol) and other catechols, causes an optical absorption shift when adsorbed onto TiO₂ nanoparticles resulting in a color change from white to yellow (see figure 1(a))^{15,16}. As in the case of catechol on TiO₂ this must be due to either a direct molecule to substrate e⁻-transfer process¹⁷, or a change in the density of states of the

combined pABA-TiO₂ system^{18,19}, since the optical absorption onset for pABA is 360 nm (3.4 eV)²⁰. The absorption onsets for anatase TiO₂ (3.2 eV) and pABA have led to their use in sunscreens¹⁵ although pABA is less widely used now due to allergy issues.

In this work, we study the adsorption mode and geometry of p-aminobenzoic acid on the anatase TiO₂(101) surface. We also characterize the density of states of pABA adsorbed on single crystal anatase TiO₂(101) in the valence band region using high-resolution valence-band photoelectron spectroscopy in order to determine the nature of the change in the size of the optical gap seen in UV-visible absorption spectroscopy measurements. Finally, we utilize Near-Edge X-ray Absorption Fine Structure (NEXAFS) spectroscopy to study the orientation of the pABA molecule on the anatase TiO₂(101) surface in order to verify that the amine group does not bond to the surface and is available for grafting of other molecules or indeed quantum dots. DFT calculations are also used to study the interaction between pABA and the anatase TiO₂ (101) surface, both to support the geometry investigations and to elucidate the optical absorption shift through study of the density of occupied and unoccupied states.

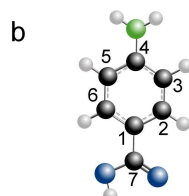


Figure 1. a) Anatase TiO₂ nanoparticles suspended in water (left) and following addition of p-aminobenzoic acid (right). b) The pABA molecule. The numbering of the carbon atoms is used for reference below.

2. Experimental and computational details.

Synchrotron radiation photoelectron spectra of clean- and pABA-dosed TiO₂ were recorded on the undulator beamline, I4, and bending-magnet beamline, D1011, at MAX-Lab, Sweden, and the undulator beamline, Antares, at Soleil, France. The anatase TiO₂ (101) single crystal (Pikem Ltd.) was prepared by repeated 1 keV Ar⁺ ion sputter and 650 °C anneal cycles until sharp (1x1) low energy electron diffraction (LEED) patterns were obtained. A survey photoelectron spectrum showed the surface to be free of contaminants. Two dosing methods were used. In the first method pABA (99.9 %, Sigma Aldrich) was packed into a Ta envelope and thoroughly outgassed in an isolated chamber at 60 °C. The evaporator temperature was then reduced to 30 °C, the sample introduced into the dosing chamber and dosed for up to 30 minutes. The base pressure of the dosing chamber was kept below 5 x 10⁻⁸ mbar and the sample was kept under vacuum between dosing and data acquisition. This process led to roughly 1 monolayer (1 ML) coverage. The second method involved pABA being placed in a sealed, evacuated port at room temperature behind a leak valve. Dosing was performed by opening the valve, which for an exposure of 10 L (1 L = 1.33 x 10⁻⁶ mbar s) resulted in approximately 1 ML coverage.

Photoelectron spectra were recorded at normal emission and are aligned on the binding energy scale referenced to a Fermi edge spectrum recorded from the Ta clips holding the sample in place, unless otherwise stated. NEXAFS spectra were recorded on beamline D1011 at MAX-Lab using a partial yield detector. The photon energy was scanned over the C K-edge monitoring all photoemitted electrons with a kinetic energy ≥ 250 eV. The sample was oriented such that the electric vector was aligned at 17° relative to the [010] azimuth. NEXAFS spectra were recorded at 10° polar angle intervals from normal incidence up to 70° from normal incidence. Spectra were divided by

the spectrum recorded from the clean surface to remove any substrate related features from the spectra. Spectra are aligned on the photon energy scale relative to the Ti L edge at 458.4 eV²¹.

To compare the adsorption of pABA on TiO₂ via the carboxylic group or via both the carboxylic and the amino group, several adsorption configurations of pABA on TiO₂ anatase (101) slabs were modelled using density-functional theory (DFT) calculations. The calculations were performed using the CRYSTAL09 code^{22,23} and employed the all-electron representation with localized Gaussian basis sets (triple valence plus polarization for Ti and O, double valence plus polarization for N, C and H - all obtained from the CRYSTAL web site²⁴) and the B3LYP hybrid density functional^{25,26}. This setup was tested in an earlier publication²⁷. Periodic TiO₂ slabs were modelled using the 2D option in CRYSTAL and contained two Ti₂O₄ layers (12 atomic layers) and (3×3) extended surface unit cells. Atoms in the lower half of the slab were fixed at their bulk positions, while the upper half of the slab and the adsorbate were allowed to relax. These (3×3) extended cells were large enough to ensure no interaction between adsorbate molecules in periodically repeated image cells. Thus, these calculations represented isolated adsorbate molecules rather than a monolayer. Following literature studies of carboxylic acids, such as formic acid^{28,29}, benzoic acid²⁷ and other aromatic carboxylic acids⁴ on the anatase (101) surface, two modes of adsorption of the carboxylic group were considered: dissociative adsorption in the bridging bidentate configuration and non-dissociative (molecular) adsorption. Additionally, for each of these adsorption modes of the carboxylic group, adsorption configurations were constructed where the amino group was also interacting with the anatase (101) surface.

Adsorption energies E_{ads} of optimized structures were calculated as:

$$E_{ads} = E_{slab+ads} - E_{slab} - E_{pABA}, \quad \text{Eq. 1}$$

where, E_{slab} is the energy of the TiO₂ slab, E_{pABA} is the energy of the isolated pABA molecule in the gas phase, and $E_{slab+ads}$ is the energy of the surface-adsorbate system. Negative values of adsorption energies correspond to favorable adsorption. Adsorption energies were corrected for the basis set superposition error (BSSE) using the counterpoise scheme³⁰.

In order to calculate NEXAFS spectra of the gas phase pABA molecule GaussView and Gaussian 03³¹ were used to produce energy minimized geometry optimized structures in order to obtain the atomic co-ordinates. These calculations were carried out using DFT B3LYP theory and the 6-31G(d,p) basis set. The co-ordinates obtained from Gaussian were then used to carry out further DFT calculations using the StoBe-deMon code³². StoBe was used to calculate the excited state X-ray absorption spectra for each C atom in the molecule individually. Summation of the individual energy calibrated spectra gives the theoretical angle-integrated NEXAFS spectrum for the molecule.

3 Results and discussion.

3.1 Photoelectron spectroscopy.

Figure 2 shows the Ti 2p, O 1s, C 1s and N 1s photoelectron spectra recorded from clean anatase TiO₂ (101) and anatase TiO₂ (101) following adsorption of a monolayer (1 ML) of pABA at a photon energy ($h\nu$) of 1000 eV. These spectra were recorded on the bending magnet beamline D1011. We define 1 ML in this case, as saturation coverage where all available five-fold coordinated Ti sites at the surface are occupied. The coverage is monitored from the relative intensity of the molecule to substrate O 1s signal³³. Figure 2a shows the Ti 2p spectra, which consist of two peaks due to spin-orbit splitting: the Ti 2p_{3/2} peak at a binding energy of 458.9 eV and the Ti 2p_{1/2} at 464.5 eV. The small peak at a binding energy of 457.4 eV is evidence of residual Ti³⁺, which for anatase TiO₂ (101) is thought to arise from subsurface oxygen vacancies³⁴. Following exposure to pABA, the Ti 2p spectrum shows no significant change apart from a rigid shift of 0.2 eV to lower binding energy, which is also observed in the O 1s spectra in figure 2b, and a small reduction in the intensity of the Ti³⁺ derived peak. The shift is due to an adsorbate induced downward band bending and has been observed following adsorption of other molecules on the TiO₂ anatase surface^{18,35}. The reduction in the intensity of the Ti³⁺ derived peak in the Ti 2p spectrum may

suggest some degree of reoxidation of surface Ti^{3+} upon adsorption of the amino acid as has been observed following adsorption of similar molecules⁴. However it is also possible that the reduction in the intensity of the Ti^{3+} peak in the Ti 2p spectrum relative to the Ti^{4+} peak is due to preferential adsorption of the molecule at O-vacancy sites, where Ti^{3+} is located³⁶.

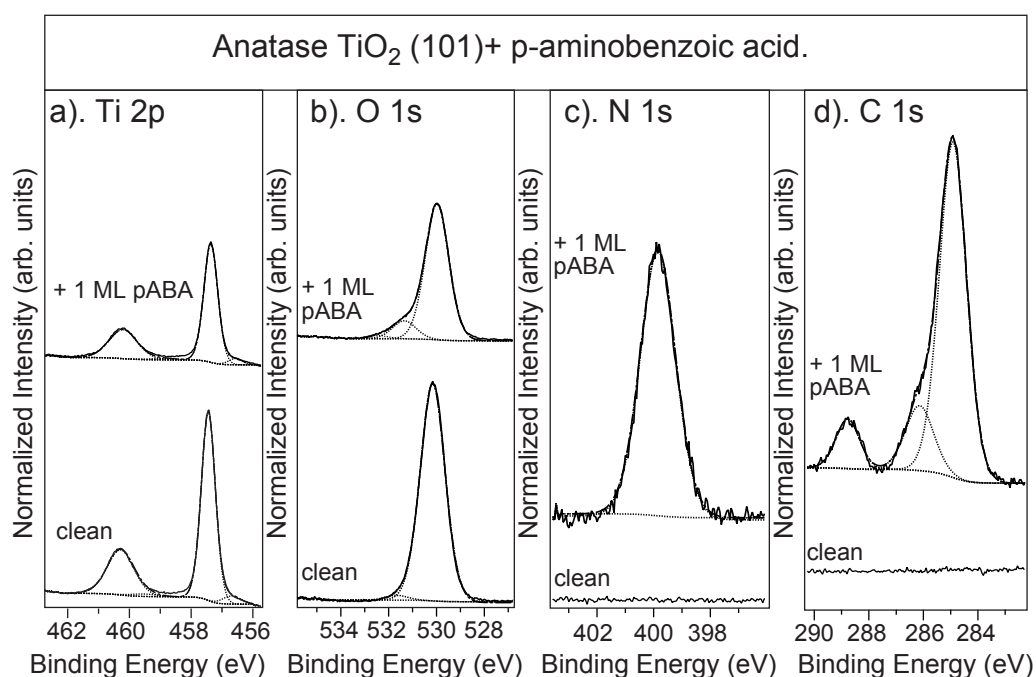


Figure 2. Core level synchrotron radiation photoemission spectra of a clean anatase TiO_2 (101) single crystal and the anatase TiO_2 (101) single crystal following adsorption of ~ 1 ML pABA . a) Ti 2p, b) O 1s, c) N 1s and d) C 1s.

Figure 2b shows the O 1s spectrum recorded from the clean TiO_2 anatase (101) surface ($h\nu = 1000$ eV) fitted with two peaks at binding energies of 530.2 eV and 531.5 eV, which are assigned to the oxide and surface oxygen close to O-vacancy sites^{37,38}, respectively. Following adsorption of around 1 ML of pABA onto the TiO_2 surface, the shoulder on the high binding energy side of the “oxide peak” is seen to increase in intensity. The O 1s spectrum can be fitted with two peaks, at energies of 530.0 eV and 531.3 eV. By comparison with the adsorption of similar molecules on TiO_2 surfaces^{4,39,40}, we assign the peak at 531.3 eV to the COO^- moiety of the amino acid.

Following adsorption of pABA on the TiO₂ (101) surface there is only a single O 1s peak associated with the molecule, strongly suggesting adsorption through both oxygen atoms in the carboxyl group following loss of the proton from the carboxylic acid group⁴⁰. The dissociation of the carboxyl group, in conjunction with studies of adsorption of other carboxylic acids on TiO₂ surfaces⁴ suggest the molecule adsorbs dissociatively on anatase TiO₂ in a bidentate configuration, via the carboxylate group. From the data here it is not possible to determine unambiguously whether this is a chelating or bridge-bonding mode. However, previous studies on adsorption of carboxylic acids on anatase and rutile TiO₂ surfaces seem to show a preference for the bidentate bridging mode^{4,5}.

The N 1s spectrum following adsorption of 1 ML pABA on the TiO₂ anatase surface is shown in figure 2c. The spectrum consists of a single peak at a binding energy of 399.9 eV consistent with the presence of NH₂^{18,41,42}. This suggests that the molecule does not form the zwitterion upon adsorption, in agreement with the adsorption of glycine on the rutile TiO₂ (011)⁴², and therefore it appears that the amine group is present as R-NH₂. This may suggest that the proton lost from the carboxylate group is adsorbed on the surface to form a surface hydroxyl species as has been observed in other carboxylic acids upon adsorption on TiO₂ surfaces.^{4,5}

The C 1s spectrum recorded following adsorption of pABA on the anatase TiO₂ (101) surface is also shown in figure 2d indicating the presence of three peaks at energies of 284.9 eV, 286.2 eV and 288.4 eV. These are assigned to carbon atoms C1, C2, C3, C5 and C6 (284.9 eV), C4 (286.2 eV) and C7 (288.4 eV), where C1-7 refer to the numbering in figure 1b. The ratio of the C 1s peak areas for the adsorbed pABA molecule is found to be 8.1:1.6:1.0. Deviations from the expected stoichiometry in similar adsorbed molecules such as this have been explained as being due to photoelectron diffraction effects⁴³, where the ordering of the overlayer and the substrate means that atoms at particular positions lead to diffraction of the photoemitted electrons, and, in turn, a reduction in the intensity of signals from electrons of a particular kinetic energy. In fact, the ring carbon/C-NH₂ ratio of 5.2:1 is in

reasonable agreement with the expected ratios for this molecule. A reduction in intensity of the carboxyl carbon derived peak is consistent with bonding to the surface via the carboxylate group, since emission from the carbon atom closest to the surface would be most susceptible to diffraction effects. Unfortunately the sample manipulator used on D1011 did not allow azimuthal rotation and energy scanned mode photoelectron diffraction measurements were not made so it is not possible to confirm that the effect is due to photoelectron diffraction. The discrepancy between the measured and expected peak ratios may of course arise from photon beam induced decomposition of the molecules with loss of CO or CO₂ from the surface. However, no changes in the relative intensities of the C 1s peaks (or O 1s) were observed over timescales of several hours under the beam.

3.2 Near Edge X-ray Absorption Fine Structure (NEXAFS).

In order to probe the unoccupied molecular states we carried out NEXAFS of the pABA powder and for a 1 ML coverage of pABA on anatase TiO₂(101). The spectra recorded from the pABA powder, and from 1 ML of adsorbed pABA with the incident synchrotron beam at 45° and 40° off normal incidence, respectively, are shown in figure 3. The 1 ML spectrum is normalized by dividing by a spectrum recorded from the clean anatase TiO₂(101) surface and that from the powder by dividing by the photon flux over the energy range of the spectrum. The large dips in both sets of experimental spectra at around 290-295 eV arise from C contamination of the beamline optics resulting in absorption at these energies. It is also noted that the 1 ML pABA-TiO₂ spectrum was recorded using a partial yield detector with a kinetic energy cut off of 250 eV on the D1011 bending magnet beamline. The spectrum from the pABA powder was recorded in constant final state mode using the Scienta analyzer to detect C KLL Auger electrons at 260 eV on the insertion device beamline ANTARES at Soleil. The large dip at around 290 eV photon energy is an artifact of the beamline. The experimental NEXAFS spectra are in good agreement with those reported by Lopez *et al.* for adsorption of pABA on Na-modified Si(100) 2 x 1 surfaces⁴⁴. Figure 3 also shows the StoBe calculated NEXAFS spectrum for the pABA molecule. The X-ray absorption spectra at

the C K-edge are calculated for each atom individually, each spectrum is

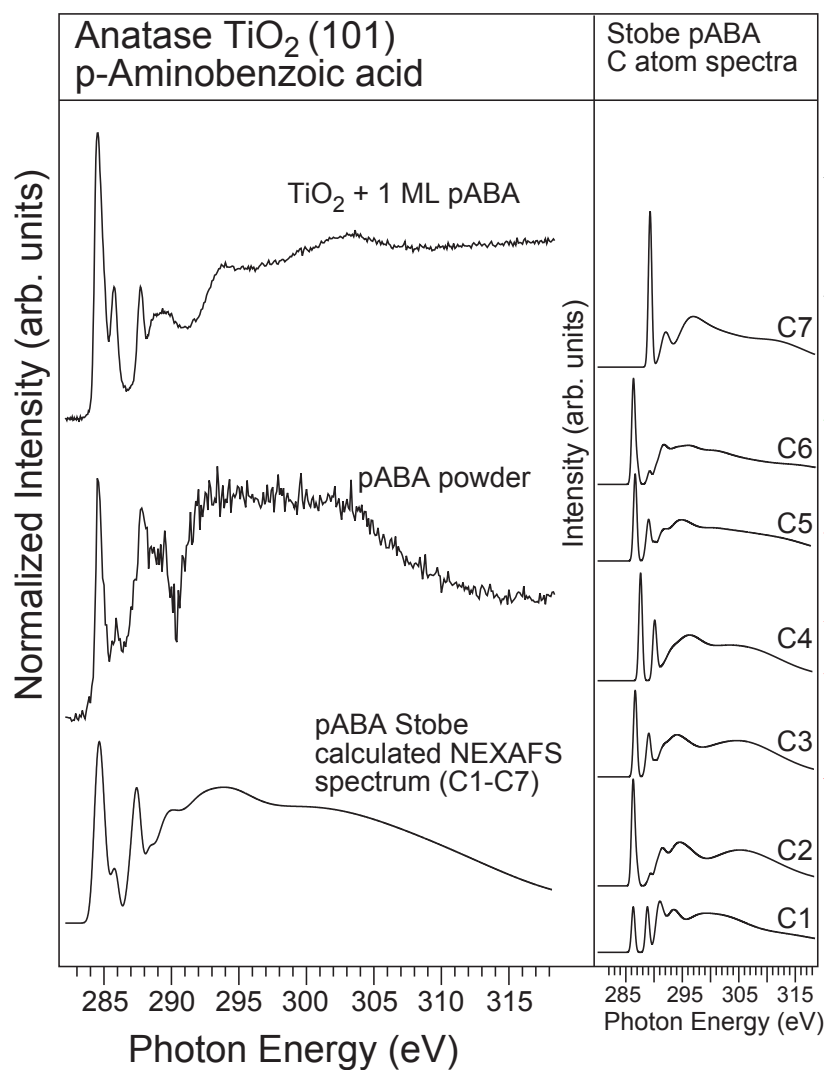


Figure 3. NEXAFS spectra recorded from pABA powder and 1 ML pABA adsorbed on an anatase TiO_2 (101) single crystal at normal emission compared to the angle-integrated StoBe calculated NEXAFS spectrum. The panel on the right shows the individual contributions of the carbon atoms. The labels C1-C7 refer to the numbers in figure 1b.

energy calibrated and convoluted with a Gaussian distribution to give a similar peak width to the experimental data before summation to give the total spectrum for the molecule. The spectra for the individual C atoms are shown in the right hand panel of figure 3. The numbering C1-C7 refers to the schematic of the molecule in figure 1 and can be used to assign the origin of the peaks seen in the experimental spectra.

The experimental and calculated spectra exhibit three clear shape resonances, at 284.5 eV, 285.9 eV and 287.8 eV in the powder and 284.5 eV, 285.8 eV and 287.7 eV in the monolayer spectrum, and 284.5, 285.8 and 287.4 eV for the calculated spectrum. These sharp features are associated with excitations from C 1s \rightarrow ring π^* orbitals in the molecule. Analysis of the calculated spectra for the individual atoms, shown in figure 3, indicate the three sharp resonances to be due to C 1s_{C-C} \rightarrow π^*_1 (284.5 eV), C 1s_{C-N} \rightarrow π^*_1 and C 1s_{C-C} \rightarrow π^*_3 (285.8 eV), and C 1s_{C=O} \rightarrow π^*_1 and C 1s_{C-N} \rightarrow π^*_3 (287.8 eV) transitions, respectively⁴⁴. In addition, careful inspection of the lowest unoccupied molecular orbital (LUMO) peak shapes for C2 and C6 show some asymmetry. This is due to excitations from C1s to the LUMO+1 (π^*_2). The broad peaks above 290 eV photon energy are assigned to C 1s \rightarrow σ^* transitions.

Figure 4 shows angle-resolved NEXAFS of the 1 ML pABA on anatase TiO₂ (101). The spectra are normalized to the absorption edge step⁴⁵. The incident radiation is oriented with electric vector at 30° \pm 5° to the $[\bar{1}01]$ azimuth. It can be seen that at normal incidence the spectra are dominated by the π^* peaks but as we move to grazing incidence the σ^* peaks become larger with a concomitant decrease in intensity of the π^* peaks. The inset shows the intensity of the C 1s_{C-C} \rightarrow π^*_1 transitions as a function of angle. The solid line is a fit based on the equations of Stöhr for a surface of 2-fold symmetry⁴⁶. The fit is consistent with the molecule adsorbing with the plane of the ring tilted at 30° \pm 15° from the normal to the surface (60° \pm 15° from the surface). The

azimuthal orientation of the ring is calculated to be at $24^\circ \pm 15^\circ$ from the

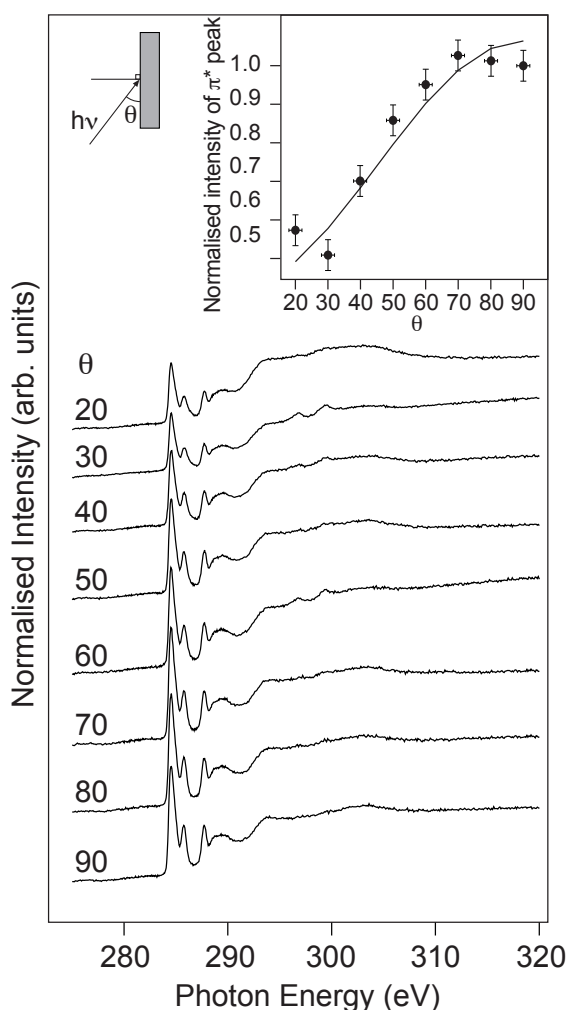


Figure 4. a) Angle resolved NEXAFS spectra recorded from the 1 ML pABA dosed anatase TiO_2 (101) single crystal. θ is the angle of incident synchrotron radiation relative to the surface. The inset shows the intensity of the dominant π^* peak as a function of angle. The line is a fit to the data using the equations of Stöhr⁴⁶.

direction of the electric vector. Since the synchrotron light was incident at 17° to the [010] azimuth we calculate the ring is aligned at an angle of $7^\circ \pm 15^\circ$ relative to the [010] azimuth. Due to the sample manipulator having no azimuthal control it was not possible to record NEXAFS spectra at differing azimuthal angles although it is clear that there is ordering of the adsorbed molecules.

3.3 DFT calculations

Although the O 1s photoelectron spectroscopy data clearly point to a bidentate adsorption mode, which suggests deprotonation of the carboxyl group, and the NEXAFS spectroscopy suggesting a tilt from an upright adsorption geometry, a number of groups have proposed that amino acids bond to TiO₂ surfaces through both the carboxylate and the amino groups⁴⁷⁻⁴⁹. Furthermore, the N 1s spectra tell us only that there is a single chemical environment for the amine nitrogen but do not exclude the possibility of the amine group interacting with the surface. To explore further whether the amino group is involved in adsorption of pABA on anatase (101), DFT calculations were carried out. Several types of adsorption configurations were explored (see supporting information). To obtain a comprehensive picture of adsorption of pABA via the amino group, different orientations of the molecule with respect to the surface crystallographic directions were tested; the amino group was adsorbed either intact or dissociatively (losing one hydrogen).

The structures studied in the DFT calculations are shown in figure 5 and the adsorption energies are collected in Table 1. 18 starting structures were considered, but only 13 optimized structures were obtained (see supporting information). The energies in Table 1 show that the structures adsorbed via only the carboxylic group are always more stable (typical adsorption energies of -1.0 to -0.8 eV) than those where the amino group is also adsorbed (adsorption energies of -0.5 eV and weaker). The exception is the zwitterion, which is very unfavorable in terms of the adsorption energy.

Among the structures that contain an adsorbed amino group, the structures with the non-dissociated NH₂ group are relatively more stable, while the structures involving a dissociated NH group have positive adsorption energies – implying that these structures are less favorable than even a desorbed pABA molecule (but desorption does not take place in the calculation because of the high energy barrier required to break these Ti-N bonds). Nevertheless, even the most stable configurations containing an adsorbed amino group are still considerably less stable than the structures that are adsorbed only via the

carboxylic group, and are therefore unlikely to exist. This adsorption via the carboxylic group but not via the amino group agrees very well with the NEXAFS and photoelectron spectroscopy results.

Label	Adsorption mode of carboxylic group	Adsorption mode of amino group	Adsorption energy, eV
<i>a</i>	dissoc.	-	-0.80
<i>b</i>	dissoc.	-	-0.24
<i>c</i>	dissoc. (zwitter-ion)	-	0.53
<i>d</i>	non-dissoc.	-	-0.96
<i>e</i>	non-dissoc.	-	-0.93
<i>f</i>	dissoc.	non-dissoc.	0.19
<i>f'</i>	dissoc.	dissoc.	1.75
<i>g</i>	non-dissoc.	non-dissoc.	-0.42
<i>g'</i>	non-dissoc.	dissoc.	0.70
<i>h</i>	non-dissoc.	dissoc.	1.00
<i>i</i>	non-dissoc.	dissoc.	0.82
<i>j</i>	non-dissoc.	non-dissoc.	-0.47
<i>j'</i>	non-dissoc.	dissoc.	0.88

Table 1. Adsorption energies of pABA on anatase (101).

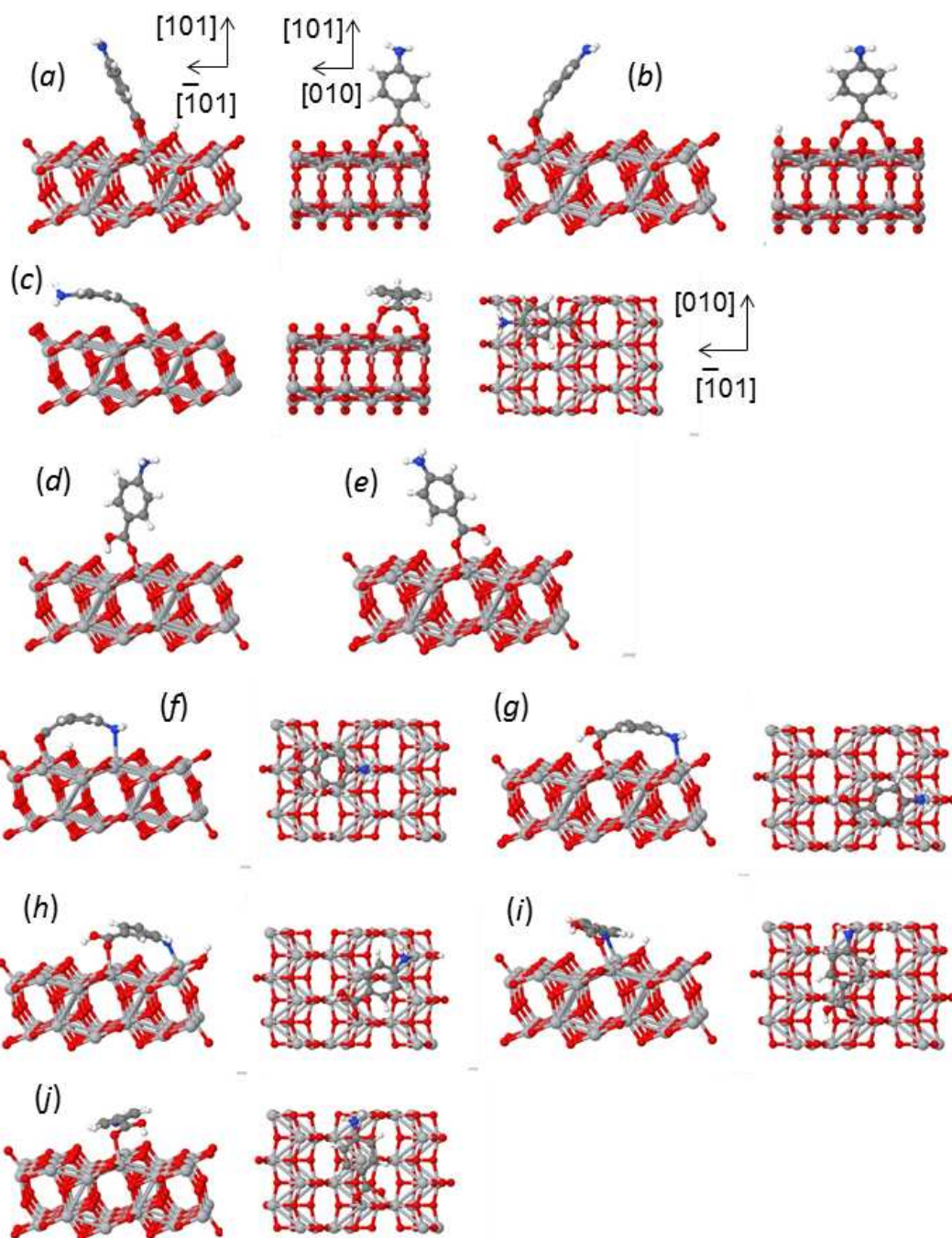


Figure 5 Adsorption configurations of pABA on anatase (101) obtained from DFT calculations: (a), (b) dissociative adsorption of the carboxylic group, (c) dissociative adsorption of the carboxylic group of the zwitterion, (d), (e) non-dissociative adsorption of the carboxylic group (the carboxylic group is either above the surface trough or above the surface Ti-O bond), (f) dissociative adsorption of the carboxylic group and non-dissociative adsorption of the amino group, (g) – (j) non-dissociative adsorption of the carboxylic group and adsorption of the amino group. Structures (f), (g), (j) can have the amino group adsorbed non-dissociatively (as shown in the figure) or dissociatively; these latter structures have higher energies (see Table 1) and are not shown in the figure.

Among the structures adsorbed only via the carboxylic group, non-dissociatively adsorbed structures have slightly larger (by ~ 0.1 eV) adsorption energies than dissociatively adsorbed structures. This is in agreement with earlier theoretical studies of carboxylic acid adsorption on anatase (101)²⁷⁻²⁹, which show that molecular adsorption is energetically favored. However, these results are in contradiction with the photoelectron spectra, which clearly show that the pABA molecule is adsorbed dissociatively – both oxygens of the molecule have the same environment. This contradiction can be explained if we consider the possibility of the full monolayer coverage of the surface by the adsorbate. If the pABA molecule is adsorbed dissociatively, at full monolayer coverage the shortest distance between atoms in neighboring molecules is approximately 3.6 Å, i.e. there is no steric clash (see figure 6(a)). On the other hand, if the molecules in the non-dissociative configuration (optimized geometries d and e in figure 5) are placed on this surface to achieve full coverage, the shortest intermolecular distance can be as short as 0.6 Å (figure 6(b)) – this clearly leads to a very strained structure. This steric clash can be avoided if the adsorbate covers every other row of 5-coordinated Ti atoms in the [010] direction, rather than every row – but this arrangement would leave under-coordinated Ti atoms free to react with other pABA molecules which can adsorb in the dissociative configuration. Therefore, even if dissociative adsorption is slightly less energetically favorable for single adsorbed molecules, it is preferable because it allows full coverage of the anatase (101) surface with the pABA adsorbate.

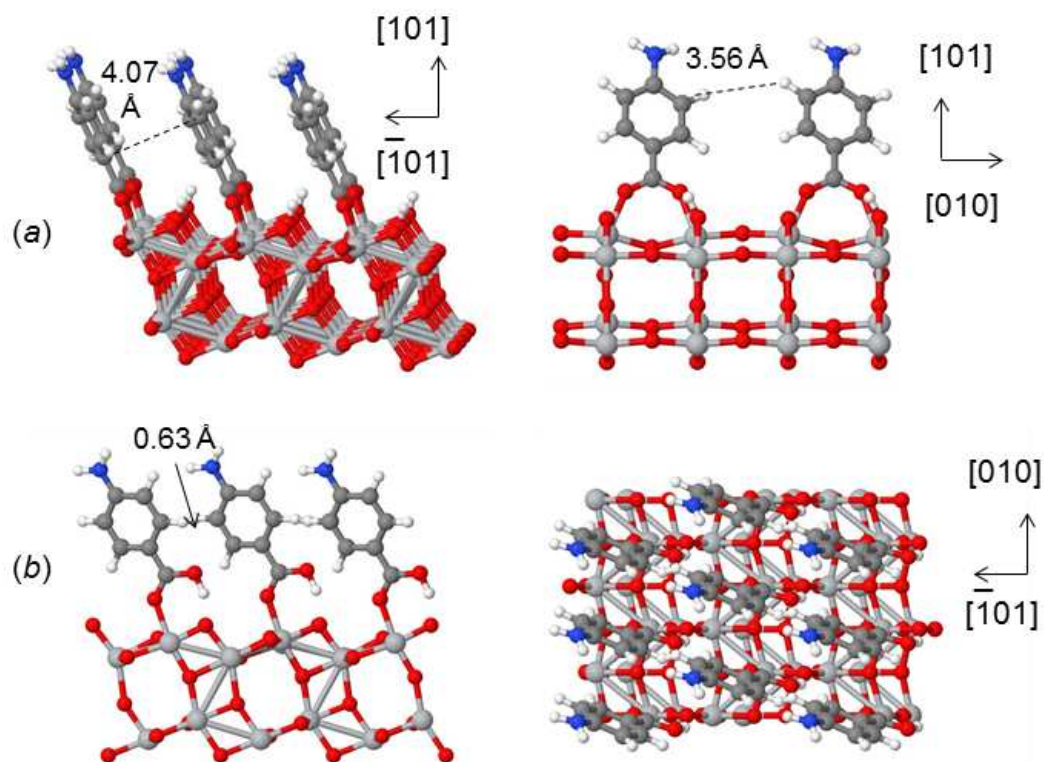


Figure 6. Models of adsorption geometries of pABA on anatase (101) at full coverage: (a) dissociative adsorption (two side views), (b) non-dissociative adsorption (side and top view).

The calculated adsorption geometry can be compared with the information on the molecular orientation given by angle resolved NEXAFS measurements. The plane of the aromatic ring in the dissociated adsorption configuration (structure (a) in figure 5) is tilted by 65.1° with respect to the surface (or 24.9° with respect to the surface normal). The plane of the ring is also twisted by 12.7° with respect to the [010] direction. These parameters are in excellent agreement with the angle resolved NEXAFS results (tilt $60^\circ \pm 15^\circ$ from the surface and twist angle of $7^\circ \pm 15^\circ$ relative to the [010] azimuth). Structure (b) in figure 5 also is compatible with experimental measurements (the calculated tilt angle is 52.7° and twist angle 13.9°), while the orientations of the molecularly adsorbed structures (d) and (e), where the molecule is approximately along the $[\bar{1}01]$ direction, are not compatible with the NEXAFS results. The adsorption geometry of the zwitterion (tilt angle 5.6° , twist angle 1.1° , figure 5(c)) is very different from the adsorption geometry of the dissociated molecule and also very different from the experimentally

determined parameters: these results confirm that the adsorbed zwitterion is not formed in experiment.

3.4 Occupied and Unoccupied Density of States Calculations and Valence Band Photoemission Spectroscopy

The density of states (DOS) has been calculated for the dissociated (deprotonated) configuration to obtain additional information on the composition of the valence and conduction band. Figure 7 shows that the calculated TiO₂ band gap is approximately 3.6 eV (slightly overestimated due to the use of the B3LYP functional); the HOMO of pABA lies approximately 1.3 eV above the top of the TiO₂ valence band and has the same energy both in the adsorbed and unbound pABA molecule. States near the bottom of the conduction band have a noticeable contribution of pABA orbitals (mainly from the oxygens and the carboxylate carbon, C7): these mixed states have no equivalent in the isolated pABA molecule whose LUMO can be seen as a sharp peak ~2.5 eV above the conduction band minimum. Therefore, in the surface-adsorbate system, the lowest-energy excitation (and optical absorption) is likely to go from the pABA HOMO to the states at the bottom of the conduction band, which have a mixed TiO₂-pABA character. The energy difference between these states and therefore the energy of this transition is approximately 2.3 eV according to the computational results. Bearing in mind that the TiO₂ band gap was overestimated by ~0.4 eV in the calculations, this energy of 2.3 eV is also likely to be overestimated, and the energy of this transition is likely to be of the order of 1.9 eV – similar to the experimental UV-Vis absorption of pABA UV vis spectroscopy of a pABA-TiO₂ nanoparticle complex (see Supporting Information fig S1).

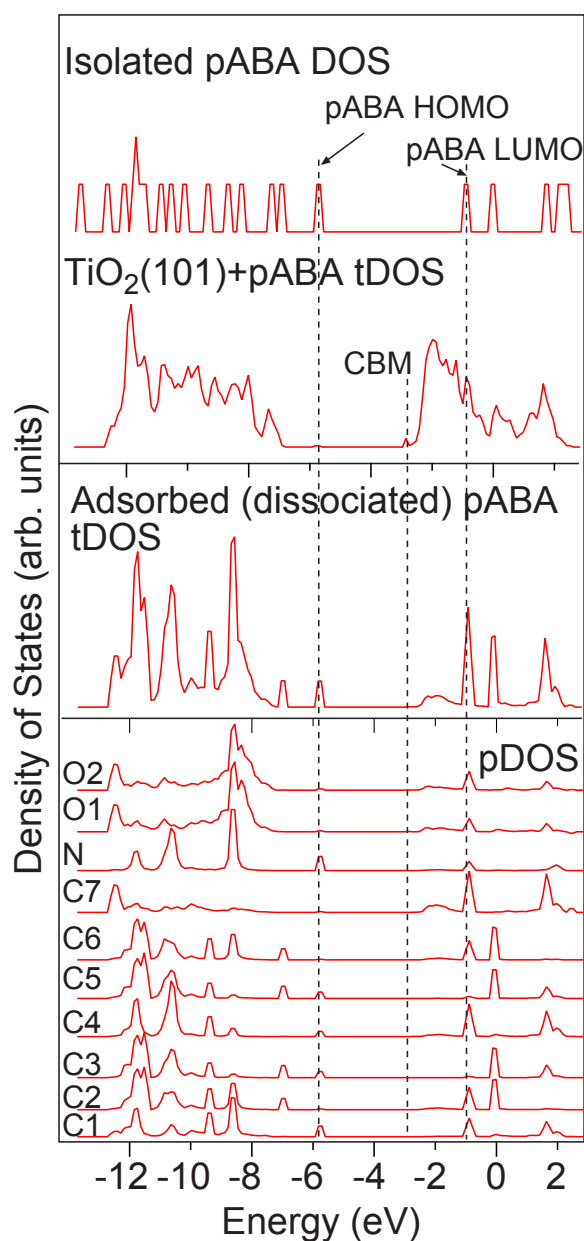


Figure 7. Total DOS (tDOS) and the contribution from individual pABA atoms (pDOS). Upper panel: total DOS for the substrate and adsorbate (scaled by the number of Ti atoms – 36 Ti atoms in the cell), and the DOS of an unbound pABA molecule; Middle panel: the contribution of the adsorbed pABA to the total DOS ; Lower panel: individual atom contributions to the adsorbed pABA DOS. The HOMO and LUMO of the isolated pABA molecule and the conduction band minimum (CBM) of the TiO_2 -adsorbate system are labeled. The vacuum level is set as the zero of energy.

The partial density of states in figure 7 show that the carboxylate carbon atom, C7, contributes to the state resulting from adsorption in the unoccupied DOS at around -2 eV with respect to the vacuum level. The two oxygen atoms also have a small contribution to this region of the unoccupied DOS. The presence of C7 states in this region may appear at odds with the StoBe calculated NEXAFS spectra. However, it should be remembered that the NEXAFS calculations are for the excited state and account for the chemically shifted carboxylate C 1s from which the electron is excited as well as the unoccupied state into which it is excited.

Figure 8 shows valence band spectra recorded from clean anatase TiO_2 (101) ($h\nu=40$ eV), and anatase TiO_2 (101) following adsorption of 1 ML pABA ($h\nu=40$ eV). The spectrum recorded from the clean anatase TiO_2 (101) surface is in good agreement with published valence band spectra recorded from this surface and at this photon energy^{21,50}. The most obvious effect of adsorbing pABA onto the TiO_2 is the location of the molecular HOMO density of states extending from the low binding energy side of the TiO_2 valence band to around 1.8 eV binding energy. Molecule-derived states in the band gap region have also been observed following catechol adsorption on this surface⁵¹. Other features due to the adsorption of the molecule are also apparent in the loss of structure in the valence band and in the appearance of new peaks at 9.4, 13.3 and 17.2 eV. The inset in figure 8 shows a difference spectrum (obtained by normalizing the clean and dosed spectra to the background and then subtracting the clean spectrum from the dosed one) compared to the occupied DOS of the adsorbed pABA molecule. The DOS calculation was placed on the binding energy scale by aligning the peaks at 5.8 and 6.9 eV in the calculation to the broad peak between 0 and 2 eV in the experimental valence band spectrum. We chose this as the normalization point since we expect the highest occupied molecular orbitals (HOMOs) to be associated mainly with the ring π -system and are therefore less likely to be perturbed by bonding to the surface. The large dip in the difference spectrum at 4.6 eV is an artifact of the subtraction process. The agreement between the calculated DOS and experimental data is rather good, although the molecular

HOMO derived peaks are much narrower than the experimentally derived peaks.

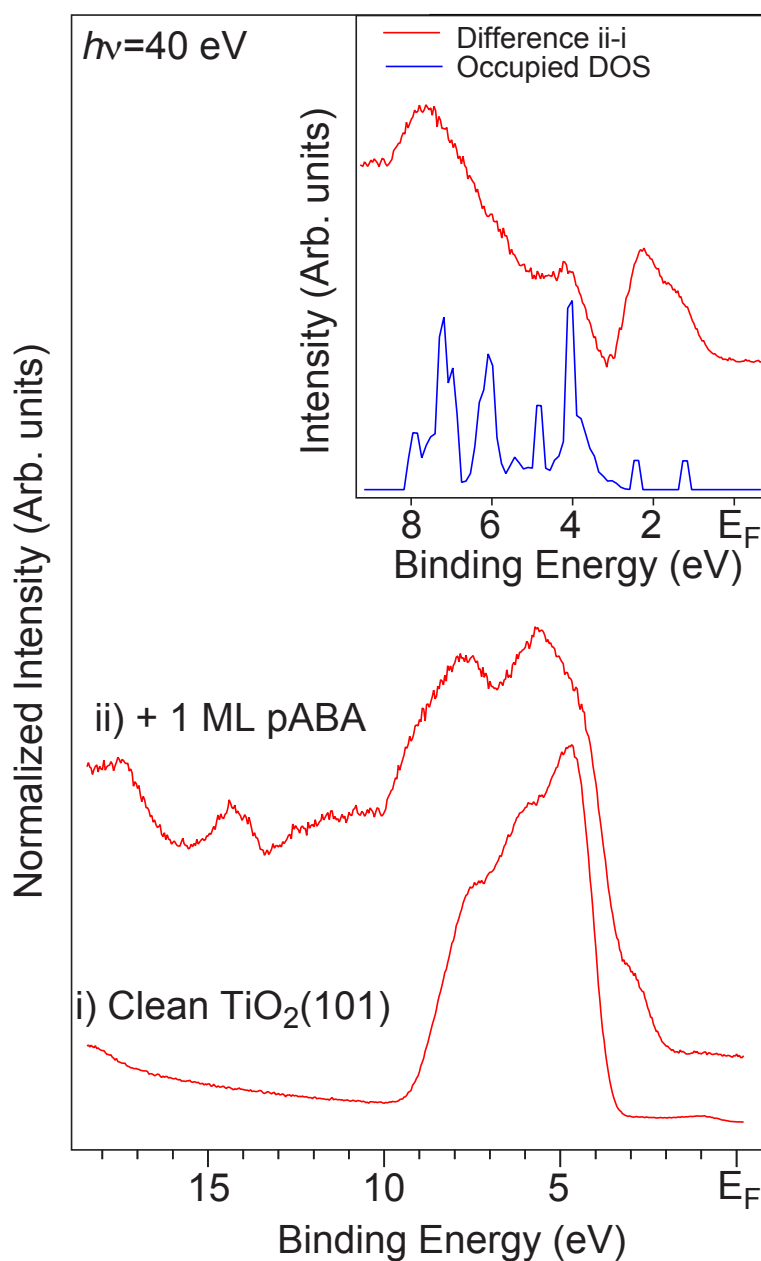


Figure 8. Valence band spectra recorded at a photon energy of 40 eV from the clean anatase TiO_2 surface, and the same surface following adsorption of 1 ML pABA. The inset shows a portion of the difference spectrum obtained by subtracting the clean surface spectrum from that of the dosed one, compared to the occupied density of states of the adsorbed pABA molecule.

In summary the valence band spectra and DOS calculations suggest that it is the position of the HOMO (ring π -bonding) derived states coupled with the presence of new molecular states in the adsorbed molecule that lead to the reduction in the optical band-gap observed in the UV-vis spectrum. The highest occupied molecular orbital to lowest unoccupied molecular orbital (HOMO-LUMO) excitation energy in the free pABA molecule is 3.4 eV. For catechol and dopamine on TiO₂ it was suggested that adsorption of the molecule onto TiO₂ leads to the presence of new molecule-substrate-derived states close to the bottom of the conduction band of the TiO₂^{18,35}. This leads to the observed change in the optical absorption onset in catechol-TiO₂ nanoparticle complexes. The DOS calculations for the adsorbed molecule support a similar process leading to the formation of the yellow pABA-TiO₂ nanoparticle “complex”. This yellow-colored complex was also observed in the work of Rahal *et al*¹⁵. It is well known that the *p*-aminobenzoate ion is also yellow, which strongly suggests the color change on adsorption is linked to electronic structure changes upon ionization of the molecule. We propose it is these changes and formation of new molecule-substrate-derived states that lead to the change in optical absorption of the pABA-TiO₂ nanoparticle? complex rather than a direct molecule to TiO₂ conduction band transfer process.

Conclusions.

p-Aminobenzoic acid was found to adsorb on the TiO₂ (101) anatase surface in a bidentate mode, most likely to be bridging between neighboring five-fold coordinated Ti atoms in the [010] direction. Core level spectra suggest the molecule adsorbs following deprotonation of the carboxyl group and the zwitterion is not formed upon adsorption. This is supported by the DFT calculations of adsorption energies, which find zwitterion formation to be particularly unstable. The amine group appears to remain intact, and oriented away from the surface at monolayer coverage and could therefore be

available for the grafting of biomolecules or light-harvesting quantum dots. Angle-resolved NEXAFS spectra and DFT-derived adsorption structures indicate the ring of the molecule to be tilted at $30 \pm 5^\circ$ to the surface normal and twisted relative to the [010] azimuth. The observed shift in the optical absorption spectrum of the pABA functionalized TiO_2 is attributed to excitations between the molecular HOMO and the presence of new molecular states, resulting from deprotonation of the adsorbed carboxyl group, close to the foot of the TiO_2 conduction band.

References

- (1) O' Regan, B.; Grätzel, M. *Nature* **1991**, *353*, 737-740.
- (2) Xie, Q.; Zhao, Y. Y.; Chen, X.; Liu, H. M.; Evans, D. G.; Yang, W. S. *Biomaterials* **2011**, *32*, 6588-6594.
- (3) Kotsokechagia, T.; Cellesi, F.; Thomas, A.; Niederberger, M.; Tirelli, N. *Langmuir* **2008**, *24*, 6988-6997.
- (4) Thomas, A.; Syres, K. *Chem. Soc. Rev.* **2012**, *41*, 4207-4217.
- (5) Pang, C. L.; Lindsay, R.; Thornton, G. *Chem. Soc. Rev.* **2008**, *37*, 2328-2353.
- (6) Diebold, U. *Surf. Sci. Rep.* **2003**, *48*, 53-229.
- (7) Jones, F. H. *Surf. Sci. Rep.* **2001**, *42*, 79-205.
- (8) Thomas, A. G.; Flavell, W. R.; Chatwin, C. P.; Kumarasinghe, A. R.; Rayner, S. M.; Kirkham, P. F.; Tsoutsou, D.; Johal, T. K.; Patel, S. *Surface Science* **2007**, *601*, 3828-3832.
- (9) Tonner, R. *ChemPhysChem* **2010**, *11*, 1053-1061.
- (10) Fleming, G. J.; Adib, K.; Rodriguez, J. A.; Barteau, M. A.; White, J. M.; Idriss, H. *Surface Science* **2008**, *602*, 2029-2038.
- (11) Rajh, T.; Saponjic, Z.; Liu, J. Q.; Dimitrijevic, N. M.; Scherer, N. F.; Vega-Arroyo, M.; Zapol, P.; Curtiss, L. A.; Thurnauer, M. C. *Nano Letters* **2004**, *4*, 1017-1023.
- (12) Kotsokechagia, T.; Zaki, N. M.; Syres, K.; de Leonardis, P.; Thomas, A.; Cellesi, F.; Tirelli, N. *Langmuir* **2012**, *28*, 11490-11501.
- (13) Mora-Sero, I.; Gimenez, S.; Moehl, T.; Fabregat-Santiago, F.; Lana-Villareal, T.; Gomez, R.; Bisquert, J. *Nanotechnology* **2008**, *19*.
- (14) Robel, I.; Subramanian, V.; Kuno, M.; Kamat, P. V. *Journal of the American Chemical Society* **2006**, *128*, 2385-2393.
- (15) Rahal, R.; Daniele, S.; Hubert-Pfalzgraf, L. G.; Guyot-Ferréol, V.; Tranchant, J.-F. *European Journal of Inorganic Chemistry* **2008**, *2008*, 980-987.
- (16) Rahal, R.; Daniele, S.; Jovic, H. *Chemical Physics Letters* **2009**, *472*, 65-68.
- (17) Persson, P.; Bergstrom, R.; Lunell, S. *Journal of Physical Chemistry B* **2000**, *104*, 10348-10351.
- (18) Syres, K.; Thomas, A.; Bondino, F.; Malvestuto, M.; Grätzel, M. *Langmuir* **2010**, *26*, 14548-14555.
- (19) Syres, K. L.; Thomas, A. G.; Flavell, W. R.; Spencer, B. F.; Bondino, F.; Malvestuto, M.; Preobrajenski, A.; Grätzel, M. *The Journal of Physical Chemistry C* **2012**.
- (20) Talrose, V.; Stern, E. B.; Goncharova, A. A.; Messineva, N. A.; Trusova, N. V.; Efimkina, M. V. UV/Visible Spectra. In *NIST Chemistry WebBook, NIST Standard Reference Database Number 69*; Linstrom, P. J., Mallard, W. G., Eds.; National Institute of Standards and Technology: Gaithersburg.
- (21) Thomas, A. G.; Flavell, W. R.; Mallick, A. K.; Kumarasinghe, A. R.; Tsoutsou, D.; Khan, N.; Chatwin, C.; Rayner, S.; Smith, G. C.; Stockbauer, R. L., et al. *Physical Review B* **2007**, *75*, 035105.
- (22) Dovesi, R.; Orlando, R.; Civalleri, B.; Roetti, C.; Saunders, V. R.; Zicovich-Wilson, C. M. *Zeitschrift für Kristallographie* **2005**, *220*, 571-573
- (23) Dovesi, R.; Saunders, V. R.; Roetti, C.; Orlando, R.; Zicovich-Wilson, C. M.; Pascale, F.; Civalleri, B.; Doll, K.; Harrison, N. M.; Bush, I. J., et al. In *CRYSTAL09 User's Manual*; University of Torino, T., Ed., 2009.

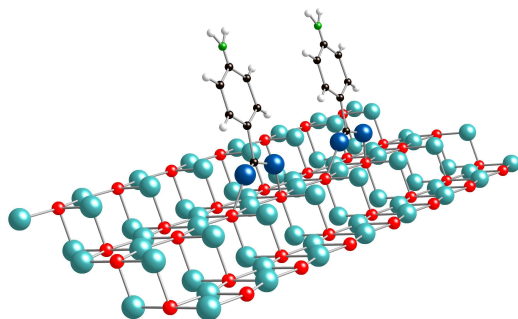
- (24) http://www.crystal.unito.it/Basis_Sets/Ptable.html. Last Accessed 07 July 2014.
- (25) Becke, A. D. *Physical Review A* **1988**, *38*, 3098-3100.
- (26) Lee, C.; Yang, W.; Parr, R. G. *Physical Review B* **1988**, *37*, 785-789.
- (27) Martsinovich, N.; Jones, D. R.; Troisi, A. *The Journal of Physical Chemistry C* **2010**, *114*, 22659-22670.
- (28) Martsinovich, N.; Troisi, A. *Physical Chemistry Chemical Physics* **2012**, *14*, 13392-13401.
- (29) Vittadini, A.; Selloni, A.; Rotzinger, F. P.; Grätzel, M. *The Journal of Physical Chemistry B* **2000**, *104*, 1300-1306.
- (30) Boys, S. F.; Bernardi, F. *Molecular Physics* **1970**, *19*, 553-566.
- (31) Frisch, M. J.; Trucks, G. W.; Schlegel, H. B.; Scuseria, G. E.; Robb, M. A.; Cheeseman, J. R.; Montgomery, J. A.; Vreven, T.; Kudin, K. N.; Burant, J. C., et al. Gaussian 03 Revision B.04; Gaussian, Inc.: Wallingford CT, 2004.
- (32) Hermann, K.; Pettersson, L. StoBe-deMon SOFTWARE, Stockholm-Berlin version 2.2 of deMon, (2006).
- (33) Schnadt, J.; O'Shea, J. N.; Patthey, L.; Schiessling, J.; Krempasky, J.; Shi, M.; Mårtensson, N.; Bruhwiler, P. A. *Surface Science* **2003**, *544*, 74-86.
- (34) He, Y. B.; Dulub, O.; Cheng, H. Z.; Selloni, A.; Diebold, U. *Physical Review Letters* **2009**, *102*, 4.
- (35) Syres, K. L.; Thomas, A. G.; Flavell, W. R.; Spencer, B. F.; Bondino, F.; Malvestuto, M.; Preobrajenski, A.; Graetzel, M. *J. Phys. Chem. C* **2012**, *116*, 23515-23525.
- (36) Jackman, M. J.; Syres, K. L.; Cant, D. J. H.; Hardman, S. J. O.; Thomas, A. G. *Langmuir* **2014**.
- (37) Thomas, A. G.; Jackman, M. J.; Syres, K. L.; Wagstaffe, M.; Li, T.-L.; Schlueter, C. *In preparation*.
- (38) Lu, G.; Bernasek, S. L.; Schwartz, J. *Surface Science* **2000**, *458*, 80-90.
- (39) O'Shea, J. N.; Luo, Y.; Schnadt, J.; Patthey, L.; Hillesheimer, H.; Krempasky, J.; Nordlund, D.; Nagasono, M.; Bruhwiler, P. A.; Martensson, N. *Surface Science* **2001**, *486*, 157-166.
- (40) Patthey, L.; Rensmo, H.; Persson, P.; Westermark, K.; Vayssieres, L.; Stashans, A.; Petersson, A.; Bruhwiler, P. A.; Siegbahn, H.; Lunell, S., et al. *Journal of Chemical Physics* **1999**, *110*, 5913-5918.
- (41) O'Shea, J. N.; Schnadt, J.; Bruhwiler, P. A.; Hillesheimer, H.; Martensson, N.; Patthey, L.; Krempasky, J.; Wang, C. K.; Luo, Y.; Agren, H. *Journal of Physical Chemistry B* **2001**, *105*, 1917-1920.
- (42) Wilson, J. N.; Dowler, R. M.; Idriss, H. *Surface Science* **2011**, *605*, 206-213.
- (43) Woodruff, D. P. *Journal of Electron Spectroscopy and Related Phenomena* **1999**, *100*, 259-272.
- (44) Lopez, A.; Bitzer, T.; Heller, T.; Richardson, N. V. *Surface Science* **2001**, *480*, 65-72.
- (45) Gutierrez-Sosa, A.; Martinez-Escolano, P.; Raza, H.; Lindsay, R.; Wincott, P. L.; Thornton, G. *Surface Science* **2001**, *471*, 163-169.
- (46) Stöhr, J. *NEXAFS Spectroscopy*; Springer-Verlag: Berlin, 2003.
- (47) Guo, Y.-n.; Lu, X.; Zhang, H.-p.; Weng, J.; Watari, F.; Leng, Y. *The Journal of Physical Chemistry C* **2011**, *115*, 18572-18581.

(48) Li, C.; Monti, S.; Carravetta, V. *The Journal of Physical Chemistry C* **2012**, *116*, 18318-18326.

(49) Szieberth, D.; Maria Ferrari, A.; Dong, X. *Physical Chemistry Chemical Physics* **2010**, *12*, 11033-11040.

(50) Thomas, A. G.; Flavell, W. R.; Kumarasinghe, A. R.; Mallick, A. K.; Tsoutsou, D.; Smith, G. C.; Stockbauer, R.; Patel, S.; Grätzel, M.; Hengerer, R. *Physical Review B* **2003**, *67*, 035110-035111 -035110-035117.

(51) Li, S. C.; Wang, J. G.; Jacobson, P.; Gong, X. Q.; Selloni, A.; Diebold, U. *Journal of the American Chemical Society* **2009**, *131*, 980-984.



TOC graphic